

LIFT AND SEPARATION CONTROL ON WIND TURBINE BLADES BY VORTICES HAVING STREAMWISE ORIENTED AXES

Václav Tesař , Jozef Kordík, Martin Daněk
Institute of Thermomechanics ASCR v.v.i., Prague

ABSTRACT

Paper describes two alternative versions of wind-turbine blade section models for tests in wind tunnel aimed at lift control at high angles of attack. They use synthetic jet (or hybrid-synthetic jet) exiting at 18 % of the chord length on the upper (suction) surface. Otherwise the two layouts are different. In version A the single synthetic jet issues from a continuous exit slit across the full span. In the other version B, a large number of small hybrid-synthetic jets exit in an anti-parallel manner (180 deg phase shift between neighbours) from a row of orifices, switched by an array of small fluidic valves inside the model. Rather surprisingly, despite the differences, the lift control in both layouts was found to be due to generation of vortices with streamwise orientation of their axes.

1. INTRODUCTION

Among other tasks, a part of the activity supported by Ministry of Education, Youth and Sport in the Research Centre 1M ("Materials and components for environment protection") is oriented towards possible ways of improving wind turbines. In the conditions prevailing in the Czech Republic, their basic shortcoming is the very slow return of the rather large necessary initial investments. What is needed to improve this situation is a reduction of the initial price. The main reason behind the high initial costs is the complexity of existing designs, in particular the expensive articulation mechanism used for adjusting the angle of attack of the rotor blades. The wind turbine would be much cheaper if its blades were rigid and need not be articulated. The present designs, with the blades are held in the hub in bearings and rotated by mechanical means, are necessary because of variability of the wind speed. At a constant shaft rotation speed, needed to drive an alternator, the effective angle of attack increases with increasing wind speed and may easily exceed the ~15 deg limit at which usual blade section stall and lose lift.

The authors investigated the possibility of controlling the lift and preventing the stall by means of synthetic (or hybrid-synthetic) jets (SyJ or HyJ) issuing on the suction surface of a rigid blades [1]. Their aim was to demonstrate absence of stall at 20 deg attack angle with relatively small power necessary for generation of SyJ or HyJ. In the SyJ case (zero time mean rate, purely alternating flow), the advantage is there are no supply tubes or cavities inside the blades needed for bringing the issuing air to the jet-generating nozzles. The disadvantage is the necessary mechanism (such as, e.g. an electrodynamic actuator [2]) for periodical expulsion of the air from a displacement cavity inside the blade alternating with return suction. Depending on the design, the actuators tend to be expensive and perhaps not absolutely reliable. From this point of view, it is advantageous to choose the HyJ case, with the jet generated by a fluidic no-moving-part oscillator [3, 4, 5, 6], inherently reliable and quite cheap. The supplied air may be available, e.g., from an inlet at the blade tip.

Apart from the mechanical simplicity of the rigid wind turbine rotor, the availability of the fast acting no-moving-part lift control can bring another benefit. It can react fast enough to suppress unsteady loads caused by inevitable wind gusts or by the blade passing past the wind turbine mast. The elimination of the unsteady loads eliminates the problem of material fatigue, currently quite serious because of the required long operational life, which is necessary as a consequence of the slow financial return rate.

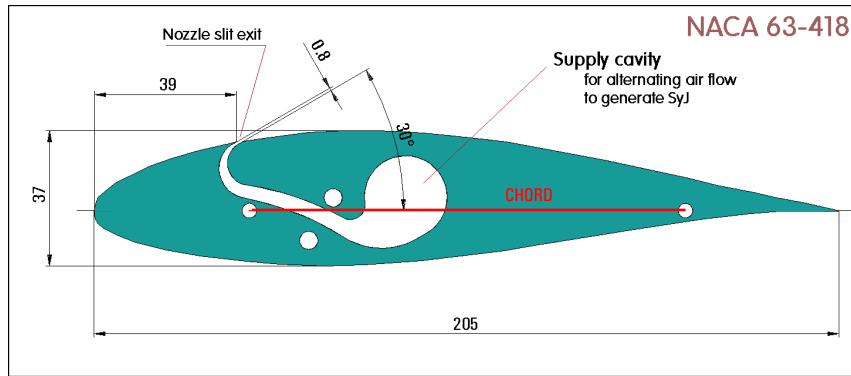


Fig. 1 The model for testing lift control by synthetic jet in the Variant A. The jet is generated in the nozzle forming a continuous slit across the full span. The somewhat strange shaped path from the central supply cavity to the nozzle was dictated by the compatibility with the end plate windows used also in Variant B.

2. TWO VARIANTS

Currently under investigation at Institute of Thermomechanics of AS CR there are two alternative versions of the models for the lift control by SyJ/HyJ. Both are of 2D geometry. They are intended for tests in the available wind tunnel, of 160 mm width and 160 mm test section height. The models span this 160 mm width between the two end windows, which are of 165 mm diameter. In the tests, the models together with the windows are to be rotated to gradually increasing attack angles up to and beyond 25 deg while the separation of the flow from the suction side will be monitored by optical means. The dimensions of the tunnel test section dictated a rather small size of the model, of 205 mm chord length (as shown in Fig. 1).

In both versions, the synthetic jet issues from the suction (top) surface of the model at identical 18 % chord length distance (measured in the chordwise direction) from the leading edge. The blowing exit channel is inclined at 30 deg direction (Fig. 1) relative to the chord.

1) **First variant A:** the generated flowfield is essentially two-dimensional. The alternating suction and blowing takes place simultaneously across the whole width of the model, Fig. 2.

2) **Second variant B:** the lift control is by an array of anti-parallel HyJ's, Fig. 3.

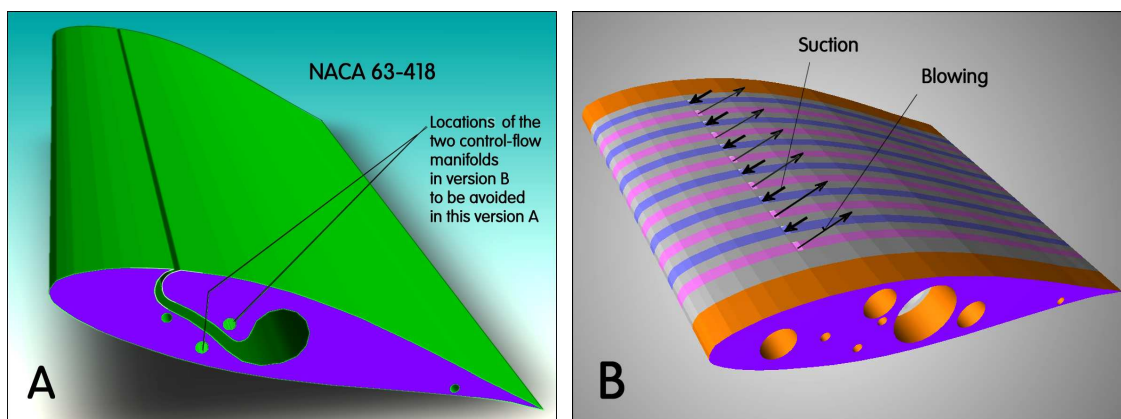


Fig. 2 (Left) The model for tests of the lift control by SyJ in the Variant A. The nozzle is a continuous slit across the full span.

Fig. 3 (Right) The other model Variant B. The row of nozzles is connected inside the model to valves switched periodically to produce the alternating outflows and inflows (shown by black arrows), of opposite direction in neighbouring exits.

The anti-parallel operation, which was in earlier tests [1] found to produce better flow-separation control effect, is a layout in which an outflow from one nozzle takes place simultaneously with suction into the neighbouring nozzles on its both sides. As shown in Fig. 3, the Variant B model is composed of a stack of thin plates — of nominal thickness 5 mm — so that the nozzles are of 0.8 x 5 mm nominal exit area.

3. VARIANT A

This variant was initially based on the idea of the separation control achieved by essentially two-dimensional effects. The whole geometry is therefore wholly two-dimensional, the model in this Variant A manufactured by electroerosive machining from a steel block, using as the tool a thin wire electrode cutting the block in its full height 160 mm. equal to the width of the wind tunnel test section.

The stall of the wind turbine blade – the flow separation from its suction surface — is expected to be eliminated by an action of sufficiently strong synthetic wall jet blown over this surface, essentially following the 1921 idea of tangential blowing by a steady wall jet proposed by Baumann [7]. The new feature is the replacement of the steady wall-jet flow by the synthetic wall-jet. Like all synthetic jet, the time-mean flow is produced due to the fluidic rectification effect [6]. The rectification converts the individual outflow "puffs" into a steady flow (initially with considerable contents of coherent vortical structures, but losing within downstream distance ~ 30 nozzle width completely the initial coherence [10]). This synthetic wall-jet attaches to the curved upper surface of the model in the Coanda attachment effect manner [8], [9], so that the exit nozzle needs not be strictly tangential relative to the surface - the 30 deg inclination relative to the chord in Fig. 1 is thus acceptable. It makes the model easier to manufacture (the thin upper lip of the nozzle is less sensitive to accidental damage), and makes possible reasonable comparisons with the basic un-blown blade when the synthetic jet is switched off (there is no surface step that the tangential nozzle would make in this regime).

Such a comparison of blown an un-blown flows, proving the feasibility of the idea of the boundary layer re-attachment, was demonstrated by numerical flowfield computations an example of the results of which are presented in Figs. 4 and 5. The flow separation from the

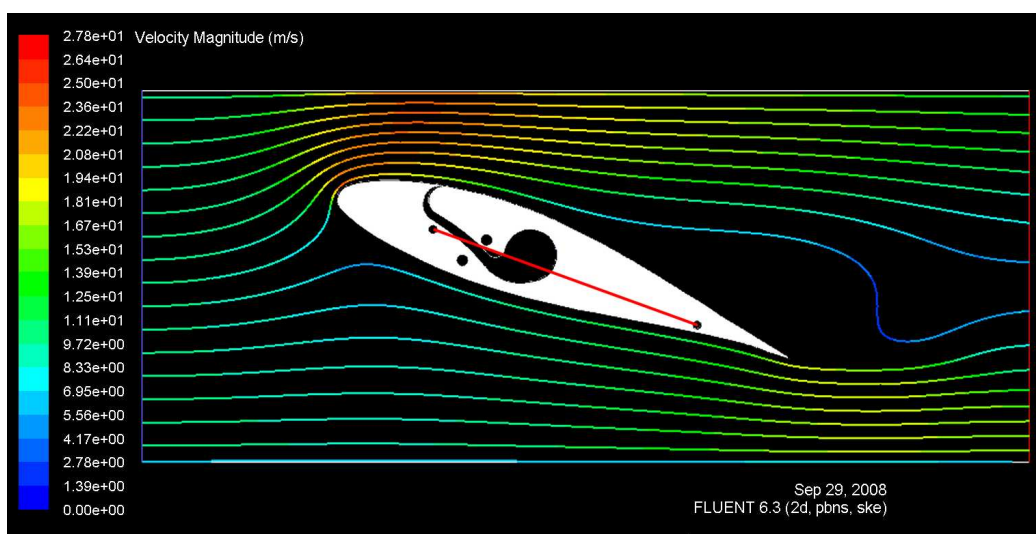


Fig. 4 Computed flowpaths obtained by two-dimensional computation of the air flow past the model in the wind tunnel test section in the Variant A. At the attack angle 20 deg with the synthetic jet inoperative, the flow separates from the model upper surface.

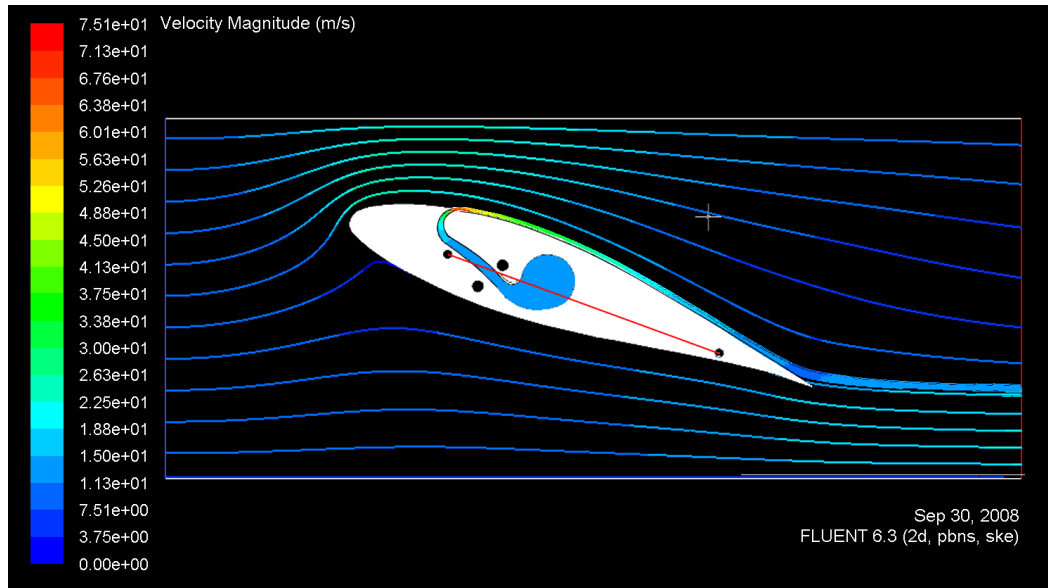


Fig. 5 Computed flowpaths demonstrate the suppression of the separation - for the same wind tunnel test with the synthetic jet on but otherwise as shown above in Fig. 4 (equal blade section, equal attack angle 20 deg, and equal wind-tunnel air velocity). Using the ideas from [10], the far-field time-mean action of the synthetic jet is simulated by a suitably adapted steady-state model of turbulence.

blade section without the blowing, as could be expected at the large angle of attack $\alpha = 20$ deg, is seen in Fig. 4. The flow re-attached at otherwise identical conditions but with the action of the synthetic wall-jet is seen in Fig. 5. The time-mean properties of the synthetic wall-jet were successfully modelled using steady-state computation with the turbulence model of the stochastic vortical motions adapted – in line with the ideas from [10] — to reasonably represent also the organised vortices. This modelling approach is especially successful for far-field behaviour, where the synthetic jet properties practically fully agree with the corresponding steady turbulent jet.

The geometry of the flow in Figs. 4 and 5 represents the conditions in the wind tunnel, with its 160 mm test section height. The pathlines would be certainly different if the blade were exposed, as it is in a wind turbine, to the wind in a practically unbounded space. The available space in the wind tunnel is evidently too small for approximating the unbounded flow. It would be necessary to make the model substantially smaller – but this was not acceptable due to compatibility with the other Variant B in which the fluidic switching valves could not be made accurately by the considered manufacturing method with the nominal accuracy of the order of 0.1 mm (claimed by the supplier, but in reality found worse).

The impossibility of modelling perfectly the free space wind turbine conditions was not considered a grave problem, because the task of the experiment was mainly a demonstration of the capability to suppress the boundary layer separation – and the tendency to the separation on the rapidly diverging space on the suction side of the blade is actually stronger than it is in the unbounded flow at the same attack angle. Thus the wind tunnel demonstration could be expected to create more unfavourable conditions, leading to a safe margin.

4. VARIANT B

The questionable feature of the variant A described above is the problem with the actuators needed to generate the alternating flow. They are difficult to stow inside the limited internal space of the blades. If they were located elsewhere – in the rotor hub, say - problems would arise with pulsation attenuation in the long ducts distributing the alternating flow.

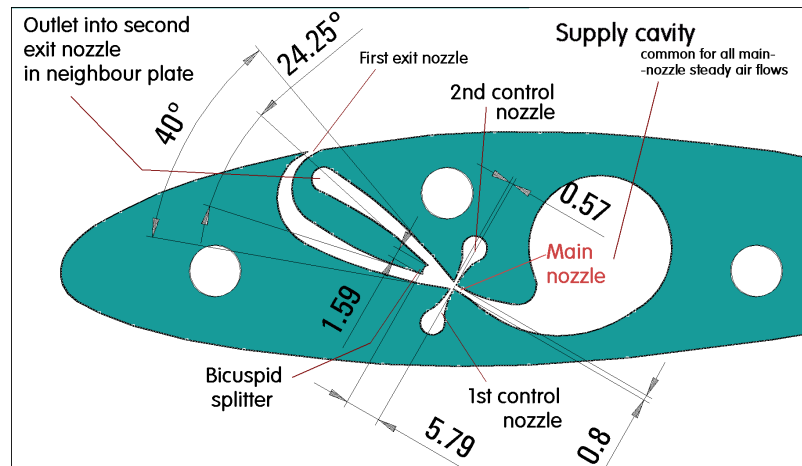


Fig. 6 Geometry of the microfluidic valve inside the Variant B model. The valve is switched to generate the alternating outflows and inflows, the latter caused by the jet-pumping entrainment into the internal jet that leaves the main nozzle.

The solution offered by the Variant B is based on the idea of placing inside the blade non-moving-part fluidic valves. These may be relatively easily manufactured as a part of the internal blade structure. The valves could even act as fluidic oscillators generating the alternating flow – but in the present case they merely serve to improve the pulse shape quality. The negative (suction) flow is generated in the valve because of the jet-pumping effect generated by the jet leaving the main nozzle. The valves are controlled by a single central oscillator. This is possible due to the valves being actually fluidic amplifiers, controllable by just small pulsating control flow. Such flow is easily distributed by relatively small cross-section ducts. The valves then need being supplied by a powerful steady flow, but this is easy to transport through the empty spaces inside the blade – coming, let us say from the blade tip, where there may be easily positioned an upstream facing air inlet. The valves generate on the spot the hybrid-synthetic jets very near to the exits, just where they are needed. The capability to shape the outflow pulses makes them well defined and near to the rectangular ideal even if the control flows are deformed by the attenuation in the long ducts. This feature may be particularly important because the experience seems to suggest a necessity of operation at a rather high frequency where the deformation of the transported pulses is considerable.

In the present case, the fluidic valves were designed as an integral part of the plates from the stack of which the model blade is composed (Figs. 3 and 7). Valve geometry, shown with some dimensions in Fig. 6, represents the scaled-down version of the valve used as the essential part of the oscillator described in [3]. The history of this successful valve geometry actually goes back as far as the early seventies of the last century [11]. As indicated in Fig. 6, the dominant characteristic dimension – the width of the supply nozzle – is less than 1 mm. This means that according to the generally accepted definition these valves fit into what is known as microfluidics [12]. The valves are made in a single operation together with the outer shape – which, as in the Variant A – corresponds to the wing section NACA 63-418, very popular section geometry for wind turbine blades. The plate with the microvalve is shown as the plate type b in Fig. 7. This plate also contains one of the synthetic-jet generating exit nozzles on its upper edge, the first nozzle n_1 . The other nozzle n_2 is made in the plate type d (Fig. 7). There are two other types of the plates, the separation plates c. They separate the valve cavities from the neighbouring plates. In Fig. 7 there is only one separation plate separation plate c_1 . This is placed in the stack between the plate b and plate d and features the transfer hole t (Fig. 7). The other separation plate c_2 is identical apart from the missing hole t. For manufacturing simplicity, all these plates were chosen to be of equal thickness, nominally 5 mm. The system of plates is set up from units. The basic unit consists of 4 plates. There is one plate b, one plate d, and two

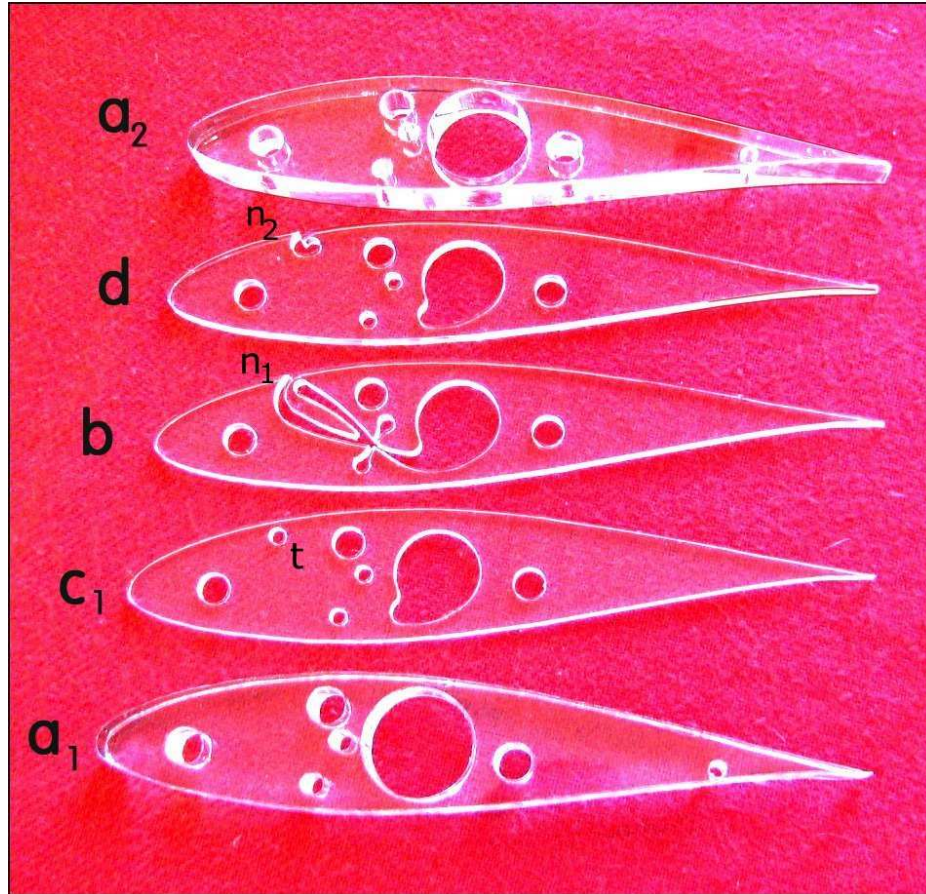


Fig. 7 Set of the plates from which the Variant B model is stacked (here not shown in their proper order in the stack). Note the two exit nozzles: n_1 in the same plate b as the microfluidic valve, and n_2 in another plate d with the separating plate c_1 between them – note the transfer hole t through which the flow pulse travels from b into d. Shown here is the original version made in transparent PMMA plates by laser cutting, later found rather imprecise.

separation plates c_1 and c_2 . As seen in Fig. 3, the 160 mm width of the test section in the wind tunnel makes possible incorporating 6 units – which means the model possesses altogether 12 exit nozzles. Apart from the units, there are in the model also two end plates 15 mm thick, one at each end of the model. The end plates are shown as a_1 and a_2 in Fig. 7. Their large thickness is necessary to hide inside them the nuts that at the end of the three bolts hold the complete stack together. The machined outer surfaces of the bolts secure the mutual position of the plates in the stack.

Initially, earlier satisfactory experience with making fluidic valves by laser cutting in polymethylmetacrylate PMMA – as described, e.g., in [3], [4] – has led to the idea of manufacturing also these plates by this technique, with the rather sophisticated outer and inner geometry (especially of the plate type b) cut in a single manufacturing operation. The set of plates pictured in Fig. 7 was made by this manufacturing technology. Unfortunately, despite the external manufacturer's claim of the 0.1 mm accuracy tolerance, the components we have received from them were found rather imprecise; especially unsatisfactory was the microvalve in the plate b which was delivered with visible asymmetry (although the fluidic valve was to be bistable, i.e. designed as symmetric).

It was, therefore, decided to use another manufacturing technology, the electroerosive machining in metal plates (Figs. 8, 9). In this case, the precision of the geometry, although not perfect, was found satisfactory. The basic 5 mm thick metal plate, however, needed machining



Fig. 8 The newer version of the plate b (Fig. 7) with the microfluidic valve, made by electroerosive machining in a steel plate.

(grinding) of both its upper and bottom surfaces before the shape could be cut. This resulted in slightly smaller than nominal metal plate thickness – actual thickness is 4.95 mm rather than the originally designed 5 mm value.

5. EXPERIMENTAL TESTS OF THE MICROVALVE

The critical new aspect in the Variant B are the microvalves. Despite their foundation on the earlier design [11], [3], [4], the small size in association with unproven manufacturing technology called for verification of their properties by laboratory tests. The tests were made on a single unit consisting of plate b (Fig. 7), plate d, the two separation plates c_1 and c_2 between them, and the pair of the end plates a_1 and a_2 (the bolts holding the model stack together had a special provision for being able to hold together only a single unit to be tested before ordering the complete set of all the plates from the external supplier). There were two sets of the tests:

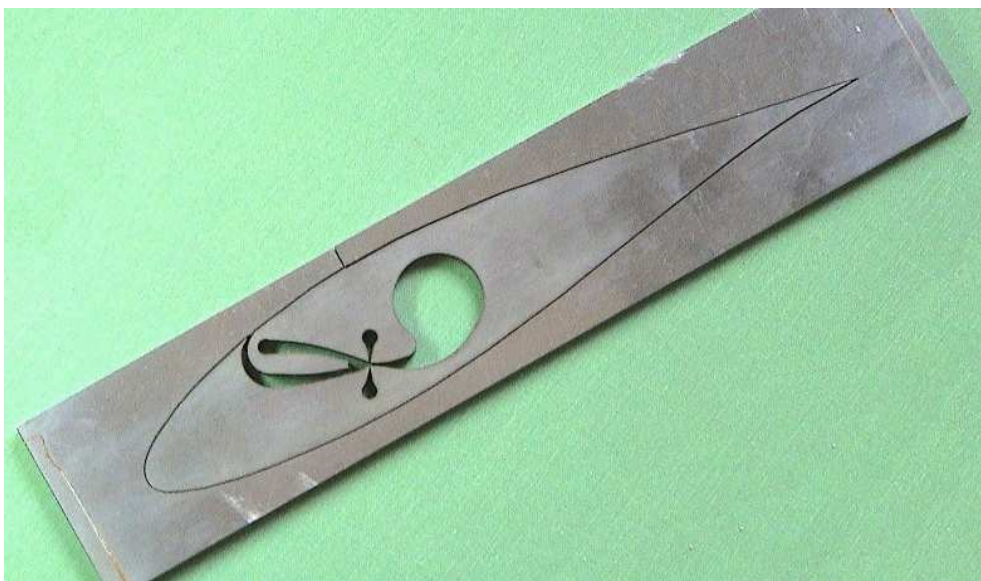


Fig. 9 The tool used in the electroerosive machining is a thin brass wire electrode moved along the contours of the manufactured shape. In this photograph the path of the wire is clearly seen.

one aimed at verifying the steady-state switching and transfer properties of the valve as predicted by numerical flowfield computations, and the other set for testing the valves in periodic unsteady regime.

5.1 Transfer characteristics tests

The layout of the tests made to verify the expected steady-state transfer characteristics is presented in Fig. 10. Steady flow of air, gradually adjusted to various flow rates measured by an orifice flowmeter, is supplied into the large central hole in the model. It should be perhaps noted that the negligibly small dependence of the price of the supplied plate on the complexity of the manufactured shapes made possible adapting the originally planned circular shape of this central hole into the shape visible in Fig. 7 in the plates d, and c₁, leading to somewhat larger flow rate and slightly lower hydraulic loss at the entry into the main nozzle. At the beginning of these tests the valve was switched so that the supplied flow (which forms the deflected jet by outflow from the main nozzle) attached to the lower attachment wall and therefore left the valve through its bottom collector, leading to the valve output Y₂ in the schematic representation in Fig. 11.

The outflows from the two exit nozzles n₁ and n₂ on the suction side of the model were monitored by velocimetric probes (it was a simple pair of Pitot probes in these steady-state tests). The control flow, the flowrate of which is measured by a rotameter, was then input into the bottom control terminal X₂ and gradually increased. Of primary interest was the control flow rate at which the switching of the valve occurs. Its value, of course, depends on the magnitude of the supply flow rate, because it is more difficult to deflect a more powerful main jet. To suppress this dependence in the pictorial representation, the results were presented in dimensionless form, with both input and output flows related to the magnitude of the supply flow (Fig. 11).

A typical switching process may be followed presented in Fig. 11 – which actually shows results of numerical computations of the valve internal flowfield. The diagram shown there is called “transfer characteristic”. It is the dependence between the control flow rate plotted on the horizontal axis and the output flow rate values on the vertical axis. In the experiment, the output flow rate is evaluated (as shown in Fig. 10) only approximately, under the idealised assumption of the output velocity w_Y everywhere the same across the whole nozzle exit area. In the computations (presented in Fig. 11) the values were known exactly. The beginning of the switching process in Fig. 11 is in the state [A], with zero control flow. The dimensionless value μ_Y of the output flow in this state is larger than 1.00, because of the jet-pumping action of the main jet, which produces suction in the other output (= in the output Y₁ in Fig. 11). The output flow passing through the terminal Y₂ is therefore the sum of the supply flow rate and this

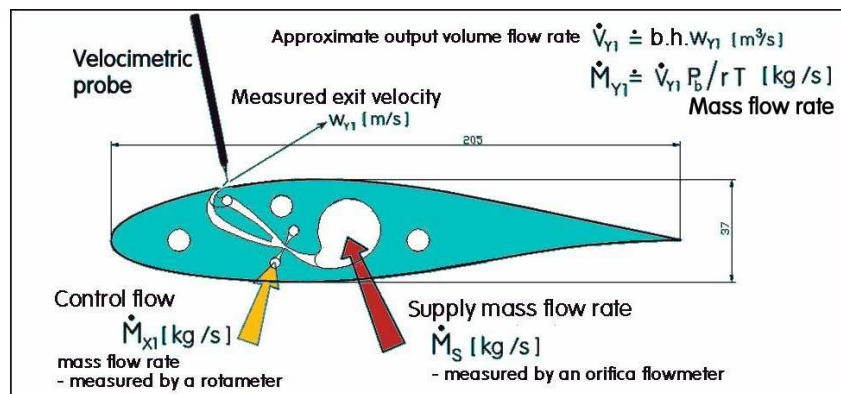


Fig. 10 Testing the operational capability of the microfluidic valve by investigations of its transfer characteristic – the dependence of the output flow rate in the SyJ generating nozzle on the control flow rate brought into one of the two control nozzles.

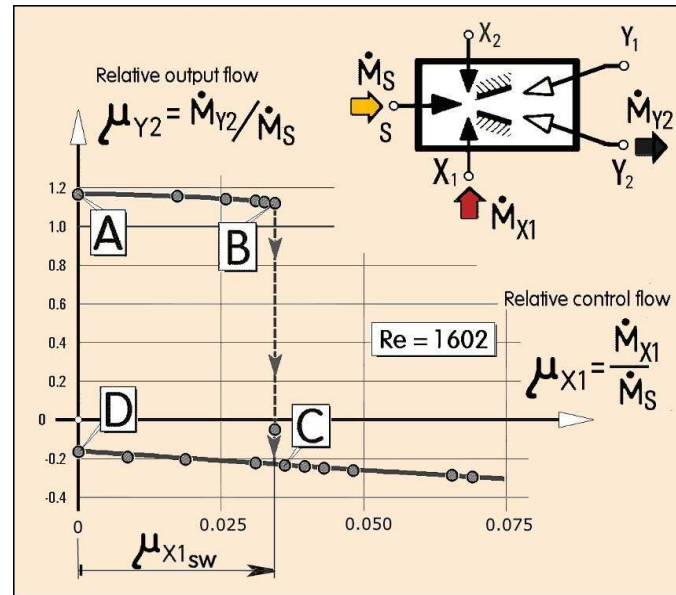


Fig. 11 Schematic representation of the fluidic valve (top right) together with an example of the transfer characteristic, in this case obtained by Fluent computations. At the beginning of the test, with no control flow, the valve has to be in the state [A] (if it were in the state [D], no switching would take place). Of particular interest is the magnitude of the relative input flow rate μ_{X1sw} at which the valve switches from [B] to [C], thus moving the output flow from Y_2 into the other output Y_1 .

amount (~ 17 % in Fig. 11) coming into the valve from atmosphere through Y_1 . When the control flow is gradually increased, the conditions in the valve gradually move from the state [A] towards the state [B]. When this state [B] is reached, the switching of the main jet into the output Y_1 takes place. In the diagram, the state [B] suddenly changes into the state [C]. The flow rate passing through the output terminal Y_2 becomes negative – this means that instead of flowing out, external air is now sucked into the valve through this terminal Y_2 . If the control flow rate is further increased, the states in the valve move further to the right from the state [C]. Nothing of importance happens: the curve as seen in Fig. 11 is slightly sloping downwards which means the suction through Y_2 is more intense, but this is not an important effect.

An important fact, however, is the hysteretic character of the change. If the control flow into the bottom control terminal X_2 is decreased, the states pass through the state [C] along the bottom branch of the curve towards the state [D], in which it remains when the control flow reduces to zero. The negative magnitude of the output suction flows through Y_2 in the state [D] equals the vertical distance between the state [A] and the value 1.00. The other control terminal X_2 is necessary for bringing in a control flow that switches the valve back into the initial state [A]. Alternatively, this return switching may be also done by a suction applied in the control terminal X_1

Experiments were performed mainly to verify the switching behaviour predicted by computations. The aim was to find the dimensionless value μ_{Xsw} of the control flow needed for the switching. The results of these experiments are presented in Fig. 12. Precise detection of the instant at which the switching takes place is rather difficult and the experiments had to be therefore repeated several times - with the resultant the data quite naturally exhibiting a considerable scatter. That is why there are the wide error bars in Fig. 12. The measurements were made at different values of the supply flow rate – which is in Fig. 12 represented by the corresponding magnitude of Reynolds number computed from the main nozzle width $b = 0.8$ mm. It seems the relative magnitude of the switching control flow decreases with increasing Reynolds number, but this is difficult to claim, considering the large data scatter. What is certain, however, is the rather small μ_{Xsw} value. From Fig. 12 it may be safely claimed that the

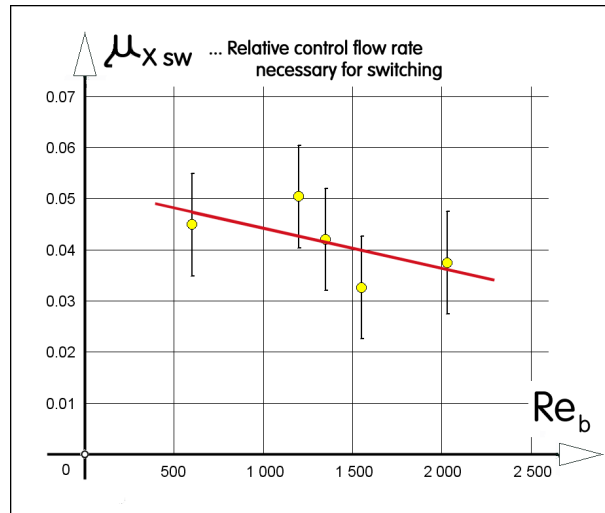


Fig. 12 Results of the experimental investigations of the switching capability of the microvalve built integrally into the model. At different supply flow rates, characterised by the values of Reynolds number, the magnitudes of the relative control flow rate $\mu_{X_{1sw}}$ were identified at which the valve switches the output from Y_2 into the other output Y_1 (Fig. 11). It is apparent that for the switching it is sufficient to apply the control flow as small as 1/20 (or perhaps even slightly less) of the switched main flow.

valve switches at the control flow rates equal to about mere 5 per cent (or perhaps even slightly less) of the supply flow rate leaving the main nozzle. In other words, the microfluidic valve was demonstrated to exhibit ~ 20- times (or perhaps even slightly higher) amplification capability. This justifies its use in the wind turbine blades, where it substantially decreases the demands on the alternating control flows to be transported through the internal cavities inside the blades.

5.2 Hot wire measurements of generated pulsation

The other set of the verification experiments focused on the dynamics of the switching. The aim was to demonstrate that the microfluidic valves can generate the synthetic jet at reasonably high repetition rates of the inlet control pulses. The shapes of the plotted dependences of exit flow velocity on time were investigated; ideally the shapes should be rectangular.

The arrangement of the test setup is presented in Fig.13. Two differences when compared to Fig. 10 are apparent. First, the control by gradually increased input flow is now replaced by the periodic action – the alternating flow generated by an electrodynamic actuator. The second difference is the replacement of the Pitot probe sensing the output velocity by a hot-wire anemometric probe capable of following fast velocity changes. Of course, the plate b (cf. Fig. 7) was in these tests not used alone (as Fig. 13 may perhaps suggest) but as a part of the complete unit, in which the plate b was supplemented by the plate d and the two separation plates c_1 and c_2 between them, the stack clamped between the end plates a_1 and a_2 . It should be mentioned that the conditions under which these tests were run were more demanding than would be the case in the actual use in the wind turbine, because the switching was here done by applying the pulses produced by the actuator only into one control nozzle terminal X_1 . There was no reverse switching action applied into the other, opposite control input X_2 . As a result, the return of the main jet to the attachment wall leading to the output Y_2 thus depended here solely on the suction, which is a less effective control action than switching by a positive control flow.

The actuator as seen in Fig. 13 was improvised from a standard, commercially available woofer loudspeaker – the final version will be probably similar, also using a proven, commercially available electrodynamic driving system. The space in front of its diaphragm was closed off by a thin metal plate thus forming there a displacement cavity from which the air was

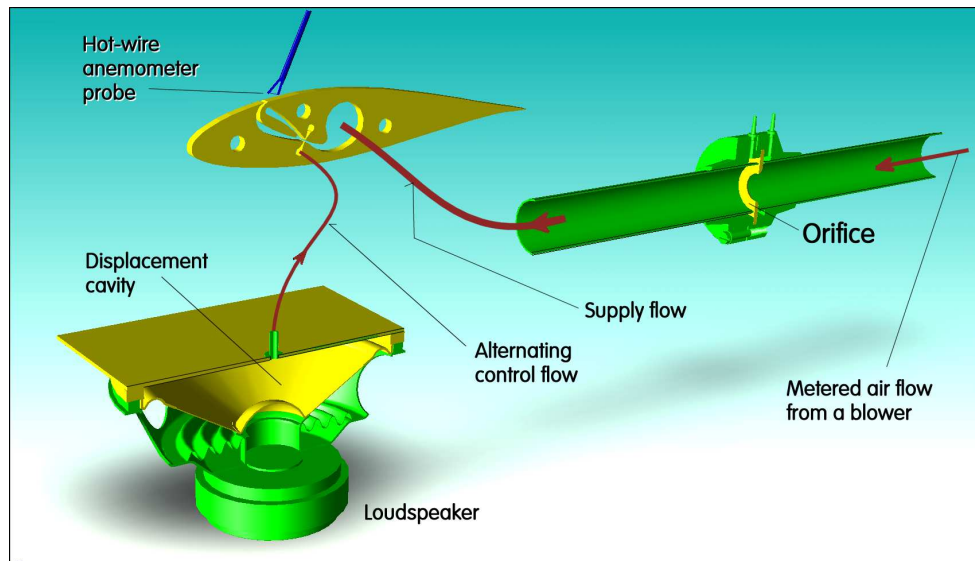


Fig. 13 Testing the response to harmonic alternating excitation. Constant time-mean power 9.3 W sinusoidal signal was fed into the actuator, the essential part of which is a woofer loudspeaker ARN-165-01/4. Its diaphragm motion displaced periodically the air from the chamber formed by covering the space in front of the diaphragm by a metal plate provided with the 3 mm dia. exit ferrule connected to the control nozzle X_1 of the microfluidic valve. The output flow from the synthetic jet nozzle is monitored by a hot-wire anemometer.

periodically displaced by the diaphragm movements. The displacement cavity was connected via the 3 mm i. d.. ferrule and by the connecting tubing with the control terminal X_2 in the plate b. The electric driving signal fed into the actuator was purely harmonic, kept at a constant power level 9.3 W (seemingly much less than the nominal output power 100 W of the loudspeaker specified by its manufacturer – but unpleasant past experience has shown that the nominal value is not applicable for continuous operation with a harmonic signal).

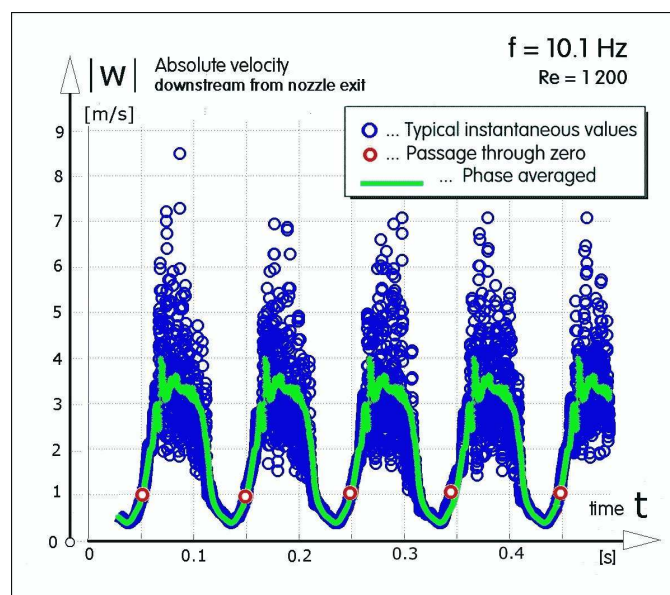


Fig. 14 An example of the measured exit pulsation as the response to the harmonic input excitation. The measured values are all positive because the used hot wire probe cannot discriminate between positive (blowing) and negative (suction) velocities. A remarkable fact is the very strong turbulence, seen in the scatter of the instantaneous values.

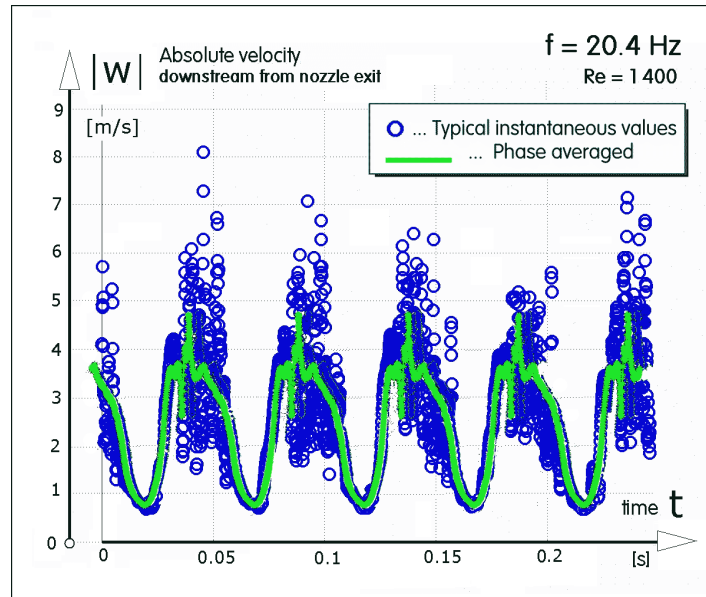


Fig. 15 Another example of the measured pulsation in the synthetic-jet generating nozzle on the top side of the model, with the internal microfluidic valve supplied with harmonic control flow at frequency 20.4 Hz. Ideally, the wave shapes should be rectangular pulses - but the actual shapes shown here are quite acceptable.

The accompanying Figs. 15 and 16 show two examples of the measurement results. The plotted quantities are the absolute velocity magnitudes, converted (using a preliminary calibration data) from the electric output signal. It is apparent that the output flow is highly turbulent – which is a useful feature as it increases the jet entrainment effect. The anemometer was used to collect a very large number of instantaneous data points, seen in blue colour in Figs. 15 and 16. Due to the high level of turbulence, the values vary significantly in the outflow phase – it should be noted that the turbulence disappears in the inflow, suction phase of the period. The collected set of data were used to perform phase averaging: values measured in a number of different pulses inside a narrow window around a particular chosen value of the phase period were averaged. The results, as the value at the particular phase angle, are plotted in green colour in Figs. 15 and 16. The conclusions from the tests performed so far is obvious: the valves do operate in the periodic switching regime and at the frequencies tested so far the waveshapes, though different from the ideal rectangles, are quite acceptable.

6. COMMON DENOMINATOR: STREAMWISE ORIENTED VORTICES

In spite of the seemingly quite different mechanisms used in the two variants of the separation control by synthetic jet – the energising of the boundary layer in Variant A, which even the authors initially considered to be an essentially two-dimensional effect, and the three-dimensional rotation along the streamwise axis (as shown in Fig. 16) in the Variant B – it was soon established that the two variants actually do have much in common.

In both cases the actual transport of momentum towards the solid surface is either driven or strongly assisted by vortices (as shown schematically in Fig. 17) oriented so that the direction of their axes locally agrees with the direction of the flowpath. In the in Variant B the rotational component of the motion is obvious. It is, of course, forced by the torque action of the pair of neighbouring anti-parallel synthetic jets. In the case of the Variant A these vortices appear due to hydrodynamic instability which was actually first discussed in reviewed literature only quite recently. The earliest known discussion in literature was by Neuendorf et al. in 2004 [14] and

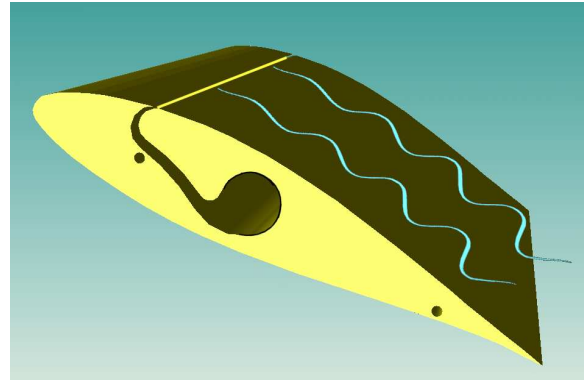
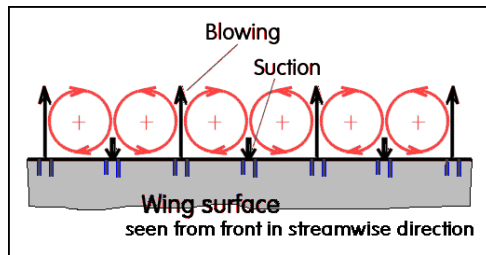


Fig. 16 (Left) An explanation for the fact that the alternating inflow and outflow pulses in neighbouring nozzles are more effective than synchronous inflows and outflows: the opposing directions of the flows produce a torque that puts the air between the two nozzles into rotation along the streamwise axis. The resultant streamwise vortices transport momentum towards the surface and inject it into the boundary layer, which would otherwise separate from the surface.

Fig. 17 (Right) The vortical motions with streamwise oriented axes actually transport momentum towards the slowly moving boundary layer on the suction surface even in the Variant A.

Then the next one by Han et al. in 2006 [15]. Recently, it was Prof. Wygnanski who made the generalisation of these individual facts and in references like [16] became the propagator of the significance of the fact that a wall-jet blown over a convex surface in principle exhibits the same instability as the Taylor-Görtler centrifugal instability due to the negative radial velocity gradient on a concave wall.

6.1 A historic reminiscence

In his studies of the Coanda-effect attachment of an air jet to a cylindrical convex curved wall [8], [9], [17], [18], the present principal author had encountered the fact – seen clearly e.g. in the accompanying Fig. 32 – that the stronger relative curvature (i.e. the shorter curvature radius relative to the nozzle exit width) leads to significantly earlier transition into turbulence at the same value of the Reynolds number. Investigations of this phenomenon he made, among other methods, by flow visualisation using gas with different refraction index issuing into air, indicated the presence of the longitudinal vortices. Among other pictures that were so far not properly published, the Figs. 20, 21 (together with Figs. 18 and 19 showing the experimental rig on which these results were obtained) certainly deserve being mentioned again in this connection. The investigated flowfield is a wall jet flowing past the convex curved wall, the surface shear stress on which was measured by an original method. The rise in the shear stress indicates the transition into turbulence – which evidently takes place at very low Reynolds numbers, at which it was earlier believed that the flow remains laminar so that the Coanda effect is too weak to lead to the attachment and deflection of the jet. Some of the pictures – in particular the spectacular here reprinted Fig. 22 - indicated quite clearly that the earlier transition is due to the presence of these disturbances in the flow. These disturbances were identified to be the vortices with streamwise axes, which (apart from being responsible for the earlier onset of the transition) also apparently transported momentum towards the wall.

Apparently, without the present author have known the fact when the experimental rig was designed, the same vortices are behind the successful application of the synthetic jet flows for separation control on the wind turbine blades. Obviously, the positive radial velocity gradient in the outer layer U of a wall jet (Fig. 23) on the convex wall leads to the same centrifugal instability as the classical case of the Taylor-Görtler instability in the negative radial gradient in the boundary layer on the concave surface.

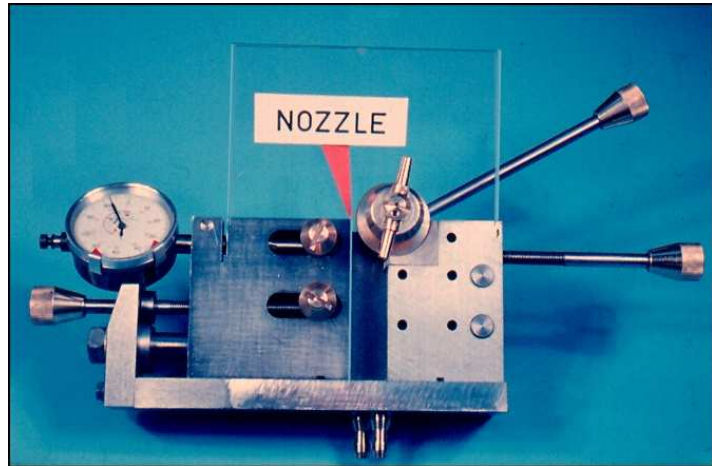
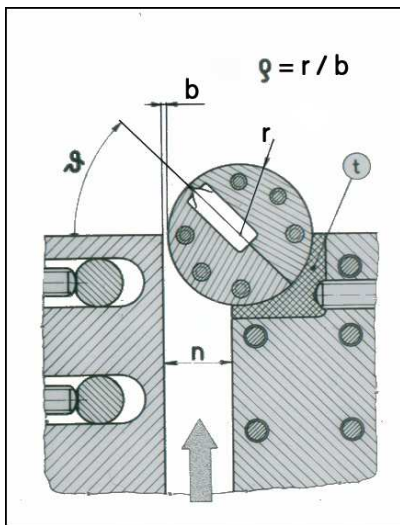


Fig. 18 (left) Drawing of the experimental rig used by the first of present authors to investigate the Coanda-effect attachment of a jet to a convex-curvature solid wall at various relative values ϱ of the curvature radius. The skin friction on the surface was investigated using the original method of the "submerged fence" – [18]

Fig. 19 (right) Photograph of the (partially disassembled) experimental rig for measurements of the distributions of the local skin friction along the cylindrical attachment surface used by the present first author in the early seventies of the last century [8], [18].

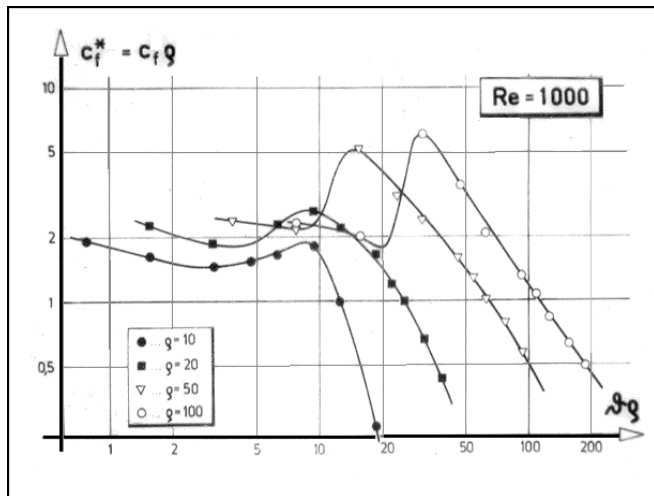
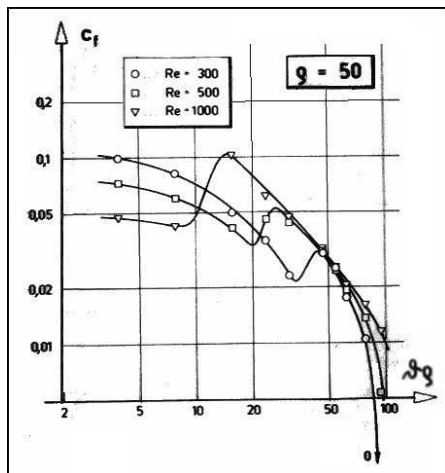


Fig. 20 (Left) The effect of Reynolds number on the distribution of the surface shear stress coefficient c_f along the cylindrical surface under the attached wall jet measured with the rig shown in Figs. 18 and 19 – the pictures are from [8]. The initial lower laminar friction decreases in the streamwise direction indicating a growing tendency towards separation. After the transition into turbulence, c_f increases and the danger of separation is postponed. The higher is the Reynolds number Re , the shorter is the distance from the nozzle to the transition.

Fig. 21 (Right) The distribution of the skin friction coefficient along the surface at a constant Reynolds number Re but different surface curvature. The shorter is the relative curvature radius ϱ , the earlier is the transition into the turbulence (demonstrated by the higher friction). Responsible for the earlier transition are the Taylor-Görtler instability vortices with streamwise oriented axes. It is a pity these important results were never properly published and only partly described in references like [8] and [9], of only local importance.



Fig. 22 Coanda-effect attachment of propane-butane wall jet issuing into air at a quite low Reynolds number – the clearly discernible : Taylor-Görtler instability vortices are visualised by Töpler's schlieren method.

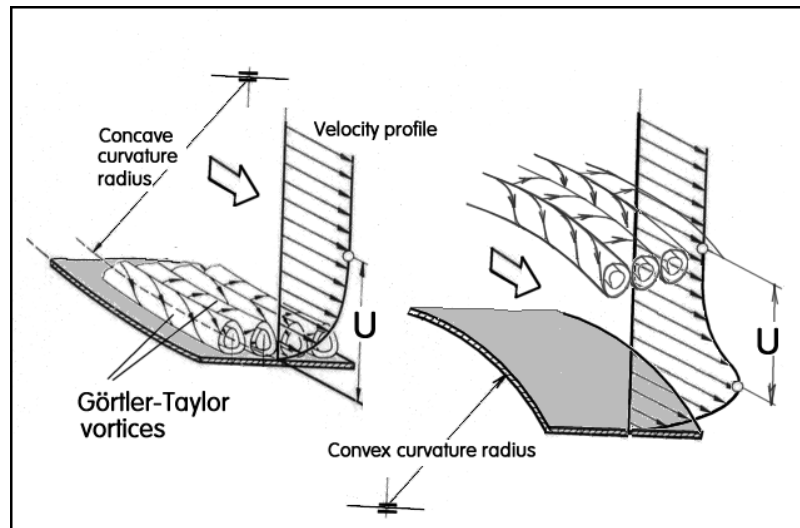


Fig. 23 A picture (unfortunately so far not properly published) drawn by the principal author in early seventies to explain the generation of the streamwise-oriented instability vortices. At left (using parts of the classical Görtler's [13] picture) the instability in the boundary layer on a concave wall, at right the instability in the outer layer U of a wall-jet on a convex wall.

It is certainly a pity that the results of the above mentioned early wall-jet investigations were never published in a journal with a wider than merely local circulation so that the role of the vortices becomes known to the scientific community only through the recent work of Prof. Wygnanski and his collaborators.

At any rate, it should be stressed that the presence of the natural instability is now known to be the reason that leads to the excellent controllability of the flow past the wind turbine blade by even very weak action of the anti-parallel synthetic jets - provided their frequency and other parameters are properly adjusted to act in line with the trend of the instability.

6. CONCLUSIONS

Initially not known to the authors, their method of separation control on wind turbine blades by synthetic (or hybrid-synthetic) jets utilises the centrifugal instability existing in the outer layer of a wall jet. This creates vortices having streamwise orientation of their axes, which suppresses the flow separation by momentum transport towards the surface. An important contribution of this proposed turbine blade layout — at least in the present wind tunnel model form — is the incorporation of integral microfluidic valves inside the blades may be done in an elegant way.

ACKNOWLEDGEMENT

The authors gratefully acknowledge the financial support obtained from the Research Project of The Ministry of Education, Youth and Sport of The Czech Republic, No. 1M06031.

References

- [1] Tesař V.: "*Fluidics Applied to Flow Control by Synthetic Jets*", Proc. of Conf. "Topical problems of Fluid Mechanics 2006", p. 171, Institute of Thermomechanics AS CR, February 2006
- [2] Tesař V., Vogel J., Trávníček Z.: "*Annular Synthetic jets for Anti-Terrorist Warfare*", Proc. of 12th International Conference on DEVELOPMENTS IN MACHINERY DESIGN AND CONTROL 2008, Nowogród, Poland, September 2008
- [3] Tesař V., Hung C.-H., Zimmerman W.: "*No-Moving-Part Hybrid-Synthetic Jet Actuator*", Sensors and Actuators A: Physical, Vol. 125, Issue 2, p. 159, 2006
- [4] Tesař V., Trávníček Z., Kordík J., Randa Z.: "*Experimental Investigation of a Fluidic Actuator Generating Hybrid-Synthetic Jets*", p. 213, Sensors and Actuators A, Vol. 138, 2007
- [5] Trávníček Z., Vít T., Tesař V.: "*Hybrid synthetic jets as the nonzero-net-mass-flux synthetic jets*", Physics of Fluids, Vol. 18, p. 081701-1, August 2006
- [6] Tesař V.: "*Configurations of fluidic actuators for generating hybrid-synthetic jets*", Sensors and Actuators A: Physical, Vol. 138, Issue 2, p. 394, doi:10.1016/j.sna.2007.05.027, 2007
- [7] Baumann, A.: "*Tragflügel für Flugzeuge mit Luftaustrittsöffnungen in der Aussenhaut*", German Patent Nr. 400806, 1921
- [8] Tesař V.: "*Experimentální vyšetřování přilnutí proudu tekutiny k zakřivenému povrchu*" (Experimental investigation of fluid jet attachment to a curved surface – in Czech), ACTA POLYTECHNICA - Práce ČVUT v Praze II, 5, 1973
- [9] Tesař V.: "*Objev lokálního minima podtlaku na stěně obtékané přilnutým proudem*" (Discovery of local pressure minimum on a wall with attached jet – in Czech), ACTA POLYTECHNICA - Práce ČVUT v Praze II, 1, 1974
- [10] Tesař V., Kordík J., Trávníček Z.: "*Similarity Solution of Synthetic Jets*", Proc. of 2nd. Int. Conf. On Jets, Wakes and Separated Flows, Berlin, Germany, September 2008
- [11] Tesař V.: "*A Mosaic of Experiences and Results from Development of High-Performance Bistable Flow-Control Elements*", Proc. of the Conf. 'Process Control by Power Fluidics', Sheffield, Great Britain, 1975
- [12] Tesař V.: "*Pressure-Driven Microfluidics*", ISBN-10: 1596931345, Artech House Publishers, Norwood, MA 02062 USA, 2007
- [13] Görtler, H.: "*On three-dimensional instability of laminar boundary layers on concave walls*", NACA Tech. Memo No. 1375, translated from German, 1940
- [14] Neuendorf, R., Lourenco, L., Wygnanski, I.: "*On large streamwise structures in a wall jet flowing over a circular cylinder*", Physics of Fluids, Vol. 16, 2004
- [15] Han, G., de Zhou, M., Wygnanski, I.: "*On streamwise vortices and their role in the development of a curved wall jet*", Physics of Fluids, Vol. 18, 2006

-
- [16] Zakharin B., Wozidlo R., Wygnanski I.: "On the Significance of Streamwise Vorticity in Turbulent Mixing and Separation Control Applications", Proc. of 2nd. Int. Conf. On Jets, Wakes and Separated Flows, Berlin, Germany, September 2008
- [17] Tesář V.: „A Region of Local Increase of Wall Static Pressure under a Curved Wall-Jet at Transitional Reynolds Numbers“, Proceedings of the Vth 'Jablonna' Conference, Published by Hungarian Academy of Sciences, Budapest, Hungary, 1974
- [18] Tesář V.: „The 'Split-Cylinder' Sensor for Skin Friction Measurement in Curved Wall-Jet Flows“ Proceedings of the Vth 'Jablonna' Conference, Published by Hungarian Academy of Sciences, Budapest, Hungary, 1974
- [19] Tesář V.: "Control of Flow Separation by Temperature Gradient", Euromech Colloquium 377 "Stability and Control of Shear Flows with Strong Temperature or Density Gradients", Praha, May, 1998
- [20] Sekerák J.: "Vizualizace proudění podél zakřivené stěny s proměnnou teplotou" (Visualisation of Flow past a Curved Wall with Variable Temperature – in Czech), Proc. of Conf. EMT06 Experimental Fluid Mechanics 2006, Liberec, December 2006

